Parkfield Fault-Zone Guided Waves: High-Resolution Delineation of the Low-Velocity Damage Zone on the San Andreas at Depth near SAFOD Site

Yong-Gang Li
[1]*Department of Earth Sciences, University of Southern California,*
Los Angeles, California 90089-0740, USA

Abstract We deployed a dense linear array of 45 seismometers across and along the San Andreas fault near the SAFOD site at Parkfield in 2003 to record fault-zone trapped waves generated by near-surface explosions and microearthquakes located within the fault zone. Observations and simulations of the fault-zone trapped waves show a ~150-200-m-wide low-velocity waveguide along the SAF, within which shear velocities are reduced by 20-40% from wall-rock velocities and the *Q* value of fault-zone rocks is 10-50, indicating the existence of a damage zone on the major plate boundary at Parkfield. The damage zone on the SAF extends across seismogenic depths to at least ~7 km and is not symmetric but extends farther on the southwest side of the main fault trace. The width and velocities of this zone delineated by fault-zone trapped waves recorded at surface arrays are consistent with the results from SAFOD drilling and logs that show high porosity and multiple slip planes in a ~200-m-wide low-velocity zone with velocity reduction of ~20-30% on the main SAF at ~3.2 km depth [Hickman, 2005]. Recently, down-hole seismic stations within the main fault zone at this depth also registered prominent fault-zone guided waves from microearthquakes occurring below, indicating that the low-velocity waveguide on the SAF extends to the deeper seismogenic level [Malin, et al., 2006].

1. Introduction

Extensive field and laboratory research, and numerical simulations indicate that the fault zone undergoes high, fluctuating stress and pervasive cracking during an earthquake [e.g., Aki, 1984; Chester et al., 1993]. While we know slip is localized on faults because of their lower strength compared to the surrounding bedrock, critical parameters remain practically unknown. For example, the friction laws are approximate [e.g., Richardson and Marone, 1999], and the magnitude of the strength reduction and its spatial extent at seismogenic depth are still not constrained well [e.g., Hickman and Evans, 1992]. However, the spatial extent of fault weakness, and the loss and recouping of strength across the earthquake cycle are critical ingredients in our understanding of fault mechanics. In order to relate present-day crustal stresses and fault motions to the geological structures formed in their past earthquake histories, we must understand the evolution of fault systems on many spatial and time scales.

Many researchers have revealed a low-velocity zone a few hundred meters to 1 km wide with velocity reductions of 10-30% and a *Vp/Vs* ratio of 2.3 surrounding the surface trace the San Andreas fault near Parkfield [e.g. Thurber *et al.,* 2003; Unsworth *et al.,* 1997; Roecker *et al.,* 2004]. The low-velocity zone is thought to be caused by intense fracturing during earthquakes, brecciation, liquid-saturation and possibly high pore-fluid pressure near the fault. Recent initial results from SAFOD drilling and borehole logs at Parkfield show a low velocity zone with high porosity a couple of hundred meters wide at the ~3 km depth, indicating a damage zone associated with the SAF [Hickman *et al.*, 2005]. Pore fluids might come up from depth and the fault-zone acts as a channel due in part to its greater permeability than adjacent blocks [Rice, 1992; Lockner *et al*., 2000]. Using fault-zone trapped waves generated by explosions and microearthquakes, and recorded at surface seismic arrays at Parkfield, Li *et al.* [1990, 1997, 2004] have delineated a ~150-200 m wide low-velocity waveguide on the SAF at seismogenic depths beneath Middle Mountain, in which shear-velocities are reduced by 20-40%. This distinct low-velocity zone is interpreted being a damage zone along the SAF accumulated in recurrence of ruptures in major earthquakes over geological time.

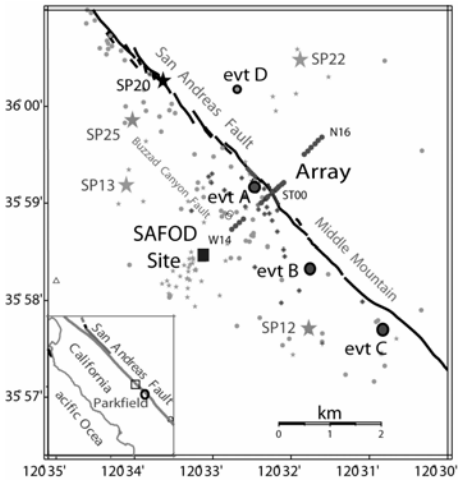

Figure 1 Map shows locations of linear seismic arrays of 45 PASSCAL RT130s (circles in line) deployed across and along the San Andreas fault near the SAFOD site (square), 5 explosions (stars) detonated by USGS, small shots (stars) and microearthquakes (dots) recorded at our array in the fall of 2003. Station ST0 in array was located on the main fault trace. Dark dots denote 37 earthquakes at different depths showing fault-zone trapped waves and are used for measurements shown in Fig. 3. Event A (2931125) is a *M*2.2 SAFOD target event occurring at ~3 km depth on Julian date R293 in 2003. Events B (2940516), C (2930452), and D (2931210) are deep earthquakes. Waveforms from them are shown in Fig. 2.

Recently, prominent fault-zone guided waves have been recorded in the SAFOD main-hole passing the SAF at 3.2 km, showing a distinct low-velocity waveguide on the SAF to deeper level [Malin et al., 2006]. In this article, we show fault-zone trapped waves recorded at a dense linear seismic array deployed across the SAF surface trace near the SAFOD site in 2003. The data from local microearthquakes occurring at different depths provide better constraints on the depth extent of the damage structure on the SAF. The results from guided waves recorded at surface arrays will help extend the direct measurements of fault-zone properties in the SAFOD main hole to a 3-D structural image of the SAF.

2. Data and Results

Seismic and geophysical surveys conducted near the SAFOD site ~15 km NW of Parkfield in 2003 have provided useful structural information before SAFOD drilling through the plate boundary. Coordinated by SAFOD PIs, we deployed a dense linear seismic array of 45 PASSCAL RT130 three-component seismometers across and along the San Andreas fault to record fault-zone trapped (guided) waves for seismic site characterization (Fig. 1). During the experiment, we recorded ~100 local earthquakes at depths between 2 and 12 km and 5 explosions in the fan-geometry detonated by the USGS. The data show prominent fault-zone trapped waves generated by the events located within the fault zone and have been used to delineate the internal damage structure and physical properties of the SAF at seismogenic depths.

Figure 2 exhibits seismograms recorded at cross-fault array for 3 microearthquakes near the SAFOD site, showing prominent fault-zone trapped waves (FZTW) with large amplitudes and long wavetrains after *S*-arrivals at stations close to the SAF main trace in a width range of ~150-200-m for events A and B occurring within the fault zone. In contrast, trapped waves are not so clear at the same stations for event C occurring 1.5 km away from the fault zone, and stations located out of the fault zone register brief body waves for 3 events. Note some seismic energy trapped within a branch fault (BF) which may connect to the main fault trace at depth. Recently, the bore seismograms recorded in the SAFOD main hole at 3.2 km depth show prominent fault-zone guided waves partitioned from the main fault to this branch fault [*Chavarria et al*., 2004; *Malin et al.,* 2006]. We also note that fault-zone trapped waves from event C occurring at ~11 km depth show much longer wavetrains of the FZTW after S-arrivals than those generated by shallow event A at ~3 km depth, indicating that the low-velocity waveguide on the SAF likely extends to deep seismogenic level. In contrast, wavetrains after *S*-arrivals at the same stations for the off-fault event D at ~9 km depth are much shorter than those from event C although two events occurred at the similar depth and distance from array.

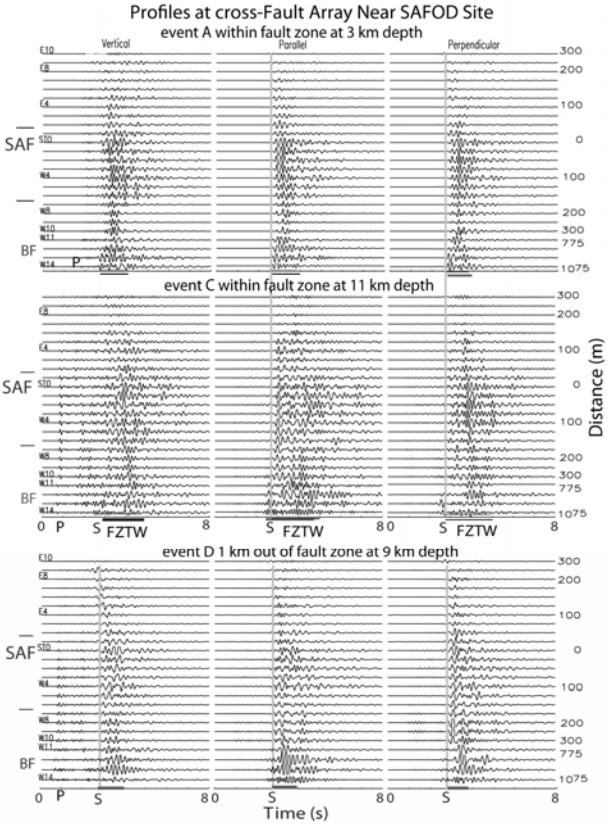

Figure 2 (a) Three-component seismograms at the cross-fault array for 3 micro earthquakes occurring within and out of the fault zone, Station names and distances from the main fault trace (SAF) are denoted. Seismograms have been (<6 Hz) filtered and plotted in a fixed amplitude scale in each plot. Prominent fault-zone trapped waves (FZTW) appear at stations between E6 and W4, indicating a ~150-200-m wide low-velocity waveguide along the SAF. Vertical lines are aligned with *S* arrivals from these events. The solid bar denotes the length of trapped wavetrains after *S*-waves. The length of FZTW from the deeper event C at ~11 km is ~2.2 s much longer that ~1.2 s length of FZTW from event A at ~3 km, indicating that the low-velocity waveguide likely extends to the deep part of seismogenic zone. In contrast, the wavetrain after *S*-arrival for the off-fault event D at the same depth of event C is much shorter than that for event C within the fault zone. Note that some seismic energy was trapped within a branch fault (BF) of the SAF.

In order to examine the depth extension of the low-velocity zone on the SAF, we used the data from 37 local earthquakes located within the fault zone at different depths with the raypath incidence angles to the array smaller than 30^{o} from vertical (Fig. 3a). Figure 3b shows seismograms and envelopes at station ST0 located on the main fault trace for 11 on-fault events at different depths near SAFOD site. *S*-arrivals for these events are aligned at 2 s. The length of fault-zone trapped wavetrains following *S*-arrivals progressively increases from ~1.2 s to ~2.2 s as the event depths increase from 2.6 km to 11.7 km. In contrast, much shorter wavetrains after *S*-arrivals with flat changes in length are registered at the same station for 11 other

events located away from the fault zone in the similar depth range. In Figure 3d, we plot the measured FZTW wavetrain lengths for 37 on-fault events and 13 off-fault events at depths between 2 km and 12 km, showing that the lengths of FZTW wavetrains at stations within the fault zone for on-fault events increase from 1.0 s to 2.2 s as the depth increases from ~2 km to ~12 km, but shorter wavetrains with flat depth-dependent changes are seen at the same stations for off-fault events. Stations located out of the fault zone registered short wavetrains after *S*-arrivals for all these events. These observations indicate that the low-velocity waveguide (damage zone) on the SAF extends across seismogenic depths to at least 7-8 km although the velocity reduction within the zone becomes smaller with depth due to the larger confined stress at greater depths.

Based on our observations of fault-zone trapped waves, we construct a velocity and *Q* model across the SAF near the SAFOD site as shown in Fig. 4d. The wall-rock velocities are constrained by tomography profiles at Parkfield [Thurber *et al.*, 2003; Roecker *et al.*, 2003]. Using a 3-D FD code [Graves, 1996], we simulated FZTW generated by explosions to determine the shallow 1 or 2 km fault zone structure, and then simulated trapped waves from earthquakes to obtain a model of the SAF with depth-variable structure at seismogenic depths. The model parameters at 3 km depth are constrained by direct measurements of the fault zone width and velocities in the SAFOD main hole [Hickman *et al*., 2005]. Figure 4 shows FD simulations of FZTW for explosion SP20 detonated within the fault zone at ~3 km north of the SAFOD site and 2 on-fault earthquakes event A and B at depths of 3 km and 7 km, respectively. The earthquake at 3 km is a SAFOD target event occurring on R293 of 2003. We obtained a good fit of synthetics to seismograms recorded at our cross-fault array. The source at 7 km depth within the fault zone generates longer FZTW wavetrains after *S*-waves than those from a source at 3 km depth, agreeable with observations, indicating our model is applicable for the fault-zone structure near the SAFOD site. We have tested finite-difference simulations for the deep event at 7 km but using a model with a low-velocity waveguide at shallower depth of 3 km. The synthetic seismograms showed a shorter wavetrain after *S*-arrivals and could not match observed long wavetrains for this deep event.

Using the fault-zone model in Fig. 4d, we simulated seismograms (Fig. 3c) at station ST0 on the main fault trace for 11 on-fault earthquakes and 11 off-fault earthquakes at depths between 3.6 km and 11.2 km for comparison with observed seismograms (Fig. 3b) for these events. The lengths of synthetic FZTW wavetrains increase with the event depth, agreeable with our observations shown in Fig. 3b. These results further verify the existence of a low-velocity waveguide (damage zone) on the SAF at Parkfield that likely extends to seismogenic depths deeper than ~7 km.

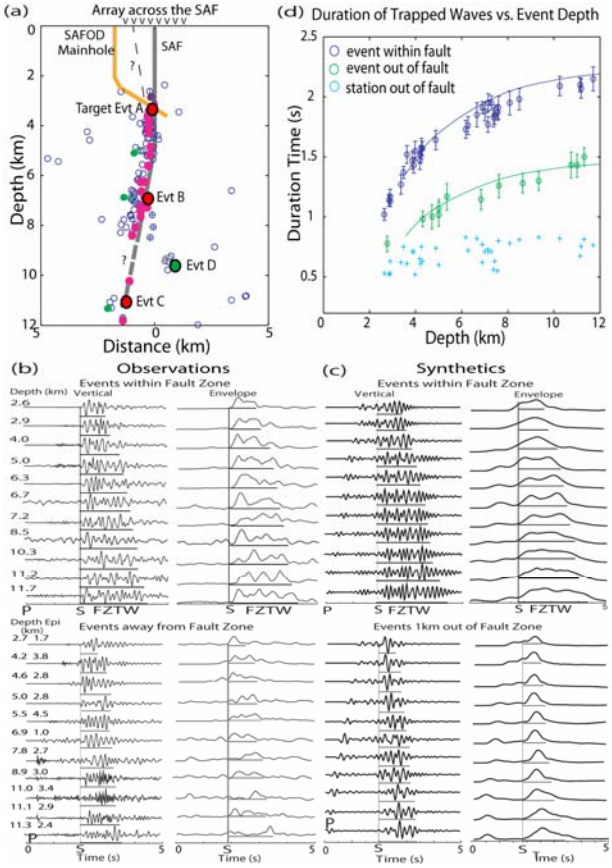

Figure 3 (a) Vertical section across the SAF and the SAFOD site shows locations of microearthquakes recorded at our seismic array in 2003. Dark (red) circles denote earthquakes showing prominent fault-zone trapped waves with long wavetrains after *S*-arrivals. Gray (green) circles denote events showing short wavetrains after *S*-arrivals. The deep part of the SAF dips toward SW at high angle. Waveforms from events A-D are shown in Fig. 2. The SAF and a branch fault (dashed lines) may connect at depth. (b) top: Vertical-component seismograms and envelopes recorded at station ST0 on the SAF main trace for 11 on-fault zone earthquakes at different depths and with the raypath incidence angle <30° from vertical show an increase in wavetrain length (marked by solid bar) of fault-zone trapped waves (FZTW) as event depths increase. *S*-arrivals for all these events are aligned in plot. Bottom: The same plot but for 11 off-fault events between the similar depths shows much shorter wavetrains after *S*-arrivals and flat changes with event depths. (c) Finite-difference synthetic seismograms and envelops at station ST0 for 11 on-fault and 11 off-fault events at different depths using the fault-zone structural model in Fig. 4d show the increasing trend of FZTW wavetrain lengths of FZTW for on-fault events agreeable with observations. In computation, the average epicentral distance of these events are 2-km from station ST0. (d) The wavetrain lengths after *S*-arrivals versus event depths for earthquakes occurring within and out of the fault zone. Each data point is averaged from measurements at 4 stations close to or far away from the fault for on-fault. Error bars are standard deviations. Curves are polynomial fits to the data. Crosses are measurements at stations located 300-m away from the fault for all these events. Plots indicate that the low-velocity zone on the SAF extends across seismogenic depths.

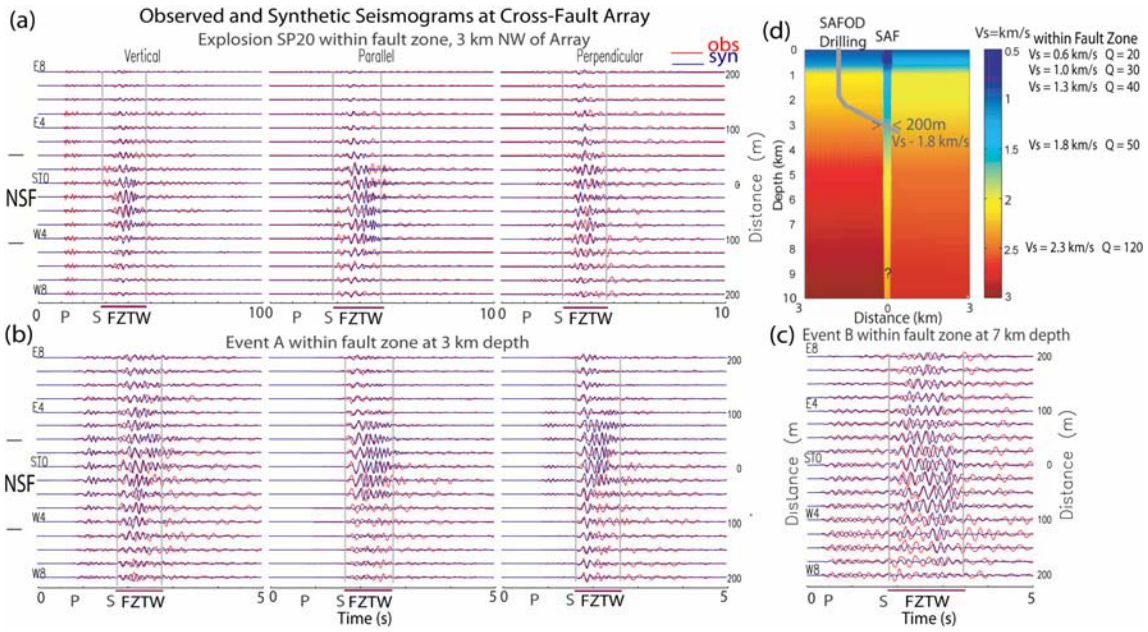

Figure 4 (a) Observed and 3-D finite-difference synthetic seismograms in three-components using model parameters shown in (d) for an explosion SP20 detonated within the fault zone, ~3 km northwest of the array. Other notations are the same in Fig. 2. (b) Same as in (a), but for the SAFOD target event A occurring at 3 km depth within the fault zone. (c) Vertical-component of observed and FD synthetic seismograms for a microearthquake event B occurring at ~7 km depth within the fault zone. *S*-arrivals are aligned at the same time for event B with event A, showing longer FZTW wavetrains for the deeper event C. A double-couple source is used for earthquakes while an explosion source is used for the shot. The FZTW wavetrains from the deeper event C is longer than that from event A. (d) Cross-fault depth sections show the structural model near the SAFOD site. Model parameters within a 100-200-m-wide low-velocity waveguide on the SAF are obtained from 3-D finite-difference simulations best fit to observed waveforms generated by explosions and earthquakes at different depths. *S* velocities within the waveguide are reduced by 25-40% from wall-rock velocities that are not symmetric at two sides of the SAF. The width and *S* velocity of the low-velocity fault zone at 3.2 km depth shown in the model are from the direct measurements in the SAFOD main hole.

3. Conclusion

Observations and modeling of fault-zone trapped waves recorded at dense linear seismic arrays deployed near the SAFOD site, Parkfield show the existence of a distinct low-velocity damage zone along the SAF and extending across seismogenic depths. The structural model for the SAF shown in Fig. 4d is still a simple one although it explains part of the data. The true structure in 3-D may be more complicated. It will be elucidated through a detailed study using the data recorded at surface and in the SAFOD main hole.

Acknowledgments. This study is supported by EarthScope Grant EAR0342277, USGS Grant NEHRP20060160, and the SCEC. Special thanks to S. Hickman, W. Ellsworth, and M. Zoback for their coordination, and E. Cochran, C. Thurber, S. Roecker, M. Rymer, R. Catchings, A. Snyder, L. Powell, B. Nadeau, N. Boness, and D. McPhee for their collaborations in our experiments at Parkfield. The author was supported by the ICDP to attend the ICDP-IODP Fault-Zone Drilling Workshop at Japan in 2006.

References

Aki, K., Asperities, barriers, characteristic earthquakes, and strong motion prediction, *J. Geophys. Res*. **89**, 5867-5872,1984.

Chavarria, J. A., P. E. Malin, E. Shalev, and R.D. Catchings. A look inside the San Andreas Fault at Parkfield through Vertical Seismic Profiling. *Science*, **302**, 1746-1748, 2004.

Chester F., J. Evans and R. Biegel, Internal structure and weakening mechanisms of the San Andreas fault, *JGR*. **98**, 771-786, 1993.

Hickman, S. H., and B. Evans, Growth of grain contacts in halite by solution-transfer: Implications for diagenesis, lithification, and strength recovery, in *Fault Mechanics and Transport Properties of Rocks*, pp. 253-280, Academic, San Diego, Cal., 1992.

Hickman, S. H., M. D. Zoback, and W. L. Ellsworth, Structure and Composition of the San Andreas fault zone at Parkfield: Initial results from SAFOD Phase 1 and 2, *EOS,* **83**, No.47, 237, 2005.

Li, Y. G., P. Leary, K. Aki, and P. Malin, Seismic trapped modes in Oroville and San Andreas fault zones, *Science*, **249**, 763-766,1990.

Li, Y. G., W. Ellsworth, C. Thurber, P. Malin, K. Aki, Observations of fault-zone trapped waves excited by explosions at the San Andreas fault California, *Bull. Seism. Soc. Am.* **87**, 210-221, 1997.

Li, Y. G., J. E., Vidale, and S. E. Cochran, Low-velocity damaged structure on the San Andreas fault at Parkfield from fault-zone trapped waves, *Geophys. Res. Lett.* **31**, L12S06, p1-5, 2004.

Lockner, D., H. Naka, H. Tanaka, H. Ito, and R. Ikeda. Permeability and strength of core samples from the Nojima fault of the 1995 Kobe earthquake, USGS Open file, Report 00-129, 147-152, 2000.

Malin, P. M., E. Shalev, H. Balven, C. Lewis-Kenedi, New fault structure on the San Andreas fault at SAFOD from P-wave tomography and fault guided waves mapping, *GRL,* in press, 2006.

Rice, J. R., Fault stress states, pore pressure distributions, and the weakness of the San Andreas fault, in *Fault Mechanics and Transport Properties of Rocks*, 475-503, 1992.

Richardson, E., and C. Marone, Effects of normal stress vibrations on frictional healing, *J. Geophys. Res*. **104**, 28,859-28,878, 1999.

Thurber, C., S. Roecker, K. Roberts, M. Gold, L. Powell, and K. Rittger, Earthquake location and 3-D fault zone structure along the creeping section of the San Andreas fault near Parkfield, CA: Preparing for SAFOD, *Geophys. Res. Lett*. **30**, 1112-1115, 2003.

Unsworth, M., P. Malin, G. Egbert and J. Booker, Internal structure of San Andreas fault at Parkfield, CA, *Geology*, 356-362, 1997.

Y.G. Li (University of Southern California, e-mail: ygli@usc.edu)

Prof. Yong-Gang Li is in Faculty of Research at University of Southern California (USC). Dr. Li is the pioneer on discovery of fault-zone trapped (guided) waves with applications to spatio-temporal characterization of active earthquake faults in 4-D. He has published 4 important papers in <<*Science*>> and <<*Nature*>> (see references) and authored more than 100 papers and scientific articles. Prof. Li has been the Principal Investigator and group leader of multiple research projects awarded by National Science Foundation (NSF), U.S. Geological Survey (USGS) and Southern California Earthquake Center (SCEC). He was graduated from Fudan University in 1960s, came to USA as a Visiting Scholar, and received his Ph.D of Seismology at USC in 1980s. Dr. Li's current research at Parkfield, called "Earthquake Capital", California is awarded by NSF-EarthScope program which is the greatest multi-disciplinary research project of earth science in USA.

References

Li, Y. G., P. C. Leary, K. Aki, and P. E. Malin, Seismic trapped modes in the Oroville and San Andreas fault zones, ***Science,*** 249, 763-, 1990.

Li, Y. G., J. E. Vidale, K. Aki, C. J. Marone, W. H. K. Lee, Fine structure of the Landers fault zone; segmentation and the rupture process, ***Science***, 256, 367-, 1994.

Li, Y. G., J. E. Vidale, K. Aki, and T. Burdette, Evidence of shallow fault zone strengthening after the 1992 M7.5 Landers, California, earthquake, ***Science***, 279, 217-, 1998.

Vidale, J. E. and **Y. G. Li** (equal contribution), Damage to the shallow Landers fault from the nearby Hector Mine earthquake, ***Nature***, 421, 524-526, 2003.